Simulated scanning tunneling microscopy images of three-dimensional clusters: $H_8Si_8O_{12}$ on Si(100)-2×1

Yunqing Chen,[1] Kevin S. Schneider,[3] Mark M. Banaszak Holl,[2,3] and B. G. Orr[1,2]

[1]*Physics Department, Harrison M. Randall Laboratory, The University of Michigan, Ann Arbor, Michigan 48109-1120, USA*
[2]*Applied Physics Program, Harrison M. Randall Laboratory, The University of Michigan, Ann Arbor, Michigan 48109-1120, USA*
[3]*Chemistry Department, The University of Michigan, Ann Arbor, Michigan 48109-1055, USA*

A scanning tunneling microscopy (STM) simulation based on the Bardeen perturbation method is used to generate simulated images of two possible chemisorption modes, monovertex and cracked cluster, for $H_8Si_8O_{12}$ on Si(100)-2×1. The tip and sample are represented by cluster models, and electronic structure calculations are performed using density-functional theory. Simulated STM images are compared to experimental STM data acquired at nominally identical tunneling conditions. The simulated STM images elucidate the preferred monovertex attachment model, in addition to providing an understanding of the cluster features and apparent vertical and lateral dimensions observed in the experimental STM data.

I. INTRODUCTION

Scanning tunneling microscopy (STM) has emerged as one of the most widely used surface characterization techniques. STM is capable of producing molecular and atomic resolution images of individually adsorbed molecules; however, the features observed often cannot be directly related to molecular geometry or structure.[1] Thus, theoretical efforts to better understand the relationship between STM images and molecular structure are necessary. A number of approaches to the chemical and physical theory of STM have been formulated.[2–8] The most widely used methods incorporate tip-sample coupling,[2–6] whereas most three-dimensional approaches are based on the scattering behavior of the tunneling electrons.[7,8] In this paper, a three-dimensional approach for simulating STM images is presented. The method employs Bardeen's perturbation model[2] and incorporates the full electronic structure of a 24-atom tip model instead of using a single atomic wave function of predefined symmetry (i.e., s wave). As a result of this geometry, the agreement between theoretical and experimental conditions is significantly improved.[6] The system modeled by these STM simulations is a chemisorbed $H_8Si_8O_{12}$ cluster on the Si(100)-2×1 surface.

The structure of $H_8Si_8O_{12}$ clusters chemisorbed on Si(100)-2×1 has been previously characterized using x-ray photoemission spectroscopy (XPS),[9,10] reflection absorption infrared spectroscopy (RAIRS),[11] and STM.[12] As a model system used to determine the XPS binding assignments for the study of amorphous silicon oxide, the veracity of many papers rests on the determination of the correct binding mode. Currently, two bonding models for the chemisorbed product have been proposed: experimental evidence has pointed towards the monovertex attachment model [Fig. 1(a)],[9–12] whereas theoretical studies have suggested the cracked cluster model [Fig. 1(b)].[13,14] Although structural assignments based upon XPS[9,10] and RAIRS[11] data have been controversial, interpretations of STM data, based largely on a comparison between experimental results and electron density maps derived from nonlocal density-functional theory (DFT) calculations, strongly support the monovertex attachment model.[12] However, the simple model previously utilized for the purposes of this comparison does not address the discrepancy between the measured experimental apparent height of the cluster and its actual geometric size. As an example, the distance between molecular features associated with the electron density of cluster oxygen atoms is larger than expected in filled-states experimental STM images. The STM simulation studies presented in this paper: (1) allow for clear interpretation of the experimental STM data, (2) provide a quantitative comparison with the experimental STM images, and (3) confirm the monovertex attachment model as the preferred cluster bonding model.

The reliable structural assignment of the chemisorption product of $H_8Si_8O_{12}$ on Si(100)-2×1 is significant for three reasons. First, the interpretation of STM images of three-dimensional molecules is still in the early stages. The assignment of observed patterns is not straightforward, and determination of molecular bonding geometries and cluster registry with respect to the underlying surface is often a challenging task. The development of high-resolution imaging
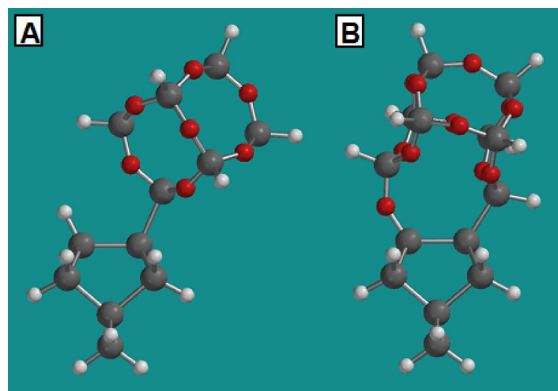

FIG. 1. (Color online) Calculated structures for the $H_8Si_8O_{12}$ adsorption models on a Si_9H_{12} silicon dimer. (a) Monovertex attachment model. (b) Cracked cluster attachment model.

techniques combined with reliable image simulation methods is critical for accurate structural interpretation. The combination of extensive studies on Si(100)-2 × 1,[15,16] $H_8Si_8O_{12}$,[17–19] and the results of the chemisorption reaction[9–14,20] make this system an excellent test bed. The second reason this system is of interest pertains to the ongoing debate regarding proper treatment of diradicals for accurately predicting chemical reactivity via quantum chemical methods. The two dangling bonds of the Si_9H_{12} cluster [representing one Si dimer of the Si(100)-2 × 1 surface] are often construed as diradicals.[21] The prediction of the cracked cluster structure was made using DFT (B3LYP, 6–31G*). However, recent reports have claimed that DFT is unable to accurately calculate force constants and energies of simple radicals such as C_5H and $C_{10}H_{10}$ within reasonable error.[22,23] It has recently been suggested that proper consideration of diradicals requires theoretical treatments, such as generalized valence bond (GVB), two-configuration self-consistent-field (TCSCF) calculations.[21] The $H_8Si_8O_{12}$ cluster itself exhibits different reaction pathways for radical versus acid/base reactions; thus, this system provides an interesting test of the theoretical models in addition to providing a probe of the radical-like or acid/base-like nature of reactions with the Si(100)-2 × 1 surface dimers. As mentioned earlier, results of the debate concerning the preferred $H_8Si_8O_{12}$ cluster bonding configuration (monovertex versus cracked cluster) have significance regarding our understanding of x-ray photoemission assignments on silicon surfaces, particularly for oxide and halogens.[24–26] Furthermore, understanding the nature of H-spherosiloxane (HSQ) clusters on Si surfaces may yield a new and interesting physical and chemical framework for a structural understanding of ultrathin silicon-oxide films and the resultant Si/SiO_2 interface.[9,24]

This paper is organized as follows: First, methods and techniques employed for the STM simulation method are briefly described. Next, simulated STM images of a single $H_8Si_8O_{12}$ cluster chemisorbed to Si(100)-2 × 1 in both the monovertex and cracked cluster bonding models are presented and discussed. Finally, a comparison between simulated and experimental STM images providing reasonable explanations regarding the experimentally observed cluster dimensions is presented.

II. THEORETICAL METHODS

A. Model

Bardeen's treatment of a tunnel junction based on perturbation theory laid the groundwork for the first theoretical STM model.[2] The tunneling current in Bardeen's formalism is expressed by

$$I = \frac{4\pi e}{\hbar} \int_0^{eV_{bias}} dE \, \rho_S(E_f - eV_{bias} + E)\rho_T(E_f + E)|M_{\mu\nu}|^2, \quad (1)$$

where ρ_S, ρ_T denote the density of states (DOS) of the sample and the tip, $M_{\mu\nu}$ is the matrix element for the transition of an electron between a wave function ψ_μ of the sample and a wave function χ_ν of the tip. Explicitly, $M_{\mu\nu}$ is defined by a surface integral over the plane within the vacuum region separating the sample and tip system

$$M_{\mu\nu} = -\frac{\hbar^2}{2m} \int_s d\vec{S} \left(\chi_\nu^* \frac{\partial}{\partial z} \psi_\mu - \psi_\nu^* \frac{\partial}{\partial z} \chi_\mu \right). \quad (2)$$

Several STM models based on Bardeen's formalism have been previously developed. Tersoff and Hamann[3] first demonstrated that tunneling current is proportional to the local density of states (LDOS) of the sample at the Fermi level measured at the tip center if the tip is represented by a single spherical *s*-type wave function. However, this treatment neglects potential geometric or chemical effects of the tip, and proves difficult for establishing a quantitative connection between experimental and theoretical data. In particular, the evanescent decay of the wave function from a single atom does not accurately match the decay anticipated from an actual tip. A more elaborate model was later developed by Hofer and co-workers, who explored extending the tip wave function via a realistic tip model.[5,6] Both the surface and tip were constructed with periodic models and represented by a set of special **k** points. Hofer and co-workers' model enhanced the field's understanding of the surface electronic structure of a crystalline STM tip and improved the ability to accurately interpret STM images.[6] The theoretical STM simulation method presented in this paper is an amalgam of Bardeen's tunneling formalism and Hofer and co-workers' model. In the present approach, both the tip and the sample are considered explicitly in cluster-type models. The main procedures are illustrated below.

First, DFT calculations were performed using commercially available quantum chemical software to derive the electronic structure of both the STM tip and sample surface.[27] Due to the cluster models used to represent the STM tip and sample surface, discrete wave functions were obtained. Upon derivation of the respective wave functions, the transition matrix elements expressed in Eq. (2) were numerically evaluated over a finite plane oriented parallel to the sample/tip model system and situated at the median distance between the apex atom of the tip and top layer of the surface atoms.[6] Taking into account that only the transition matrix elements with $\rho_S(E_f - eV_{bias} + E)\rho_T(E_f + E) \neq 0$ have significant contributions to the final tunneling current, the finite integral expressed by Eq. (1) was obtained by summing the wave functions of samples and tips with $E_\mu - eV_{bias} = E_\nu$ in the energy interval eV_{bias} near the Fermi level to evaluate the tunneling current. With these conditions, only certain wave functions near the Fermi level (sometimes termed "frontier orbitals") are included in the calculation. Considering that experimental STM data of $H_8Si_8O_{12}$ clusters on Si(100)-2 × 1 was acquired at room temperature,[12] the wave functions to be included in the calculation expressed by Eq. (1) were assumed to be broadened by 0.1 eV (the value of $3k_BT$ at 300 K). Finally, since experimental STM data is typically obtained at a constant tunneling current, it was necessary to convert the simulated images, initially generated at a constant height, to constant current images. Thus, calculations of a molecular system were performed for a range of constant heights and the results were utilized to logarithmically interpolate a constant current image.[28]

This method proves far less computationally taxing than those based on scattering theories that require individual cal-
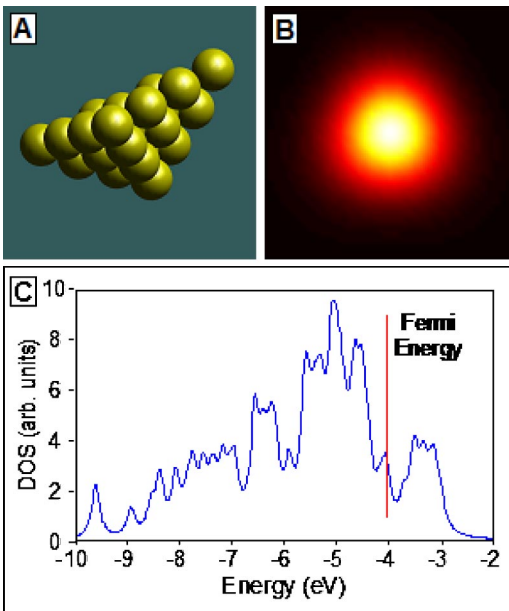
FIG. 2. (Color online) (a) The cluster model of the STM tip comprised of 24 tungsten atoms arranged in four layers in the (111) direction (lattice constant 3.19 Å). (b) LDOS plotted in the plane 3 Å above the nuclear core of the tip apex atom over an integrated energy range of 1.5 eV (from $E_f-1.5$ eV to E_f). (c) The calculated DOS of the tip cluster model.

culations to be performed for every tip position.[7,8] Instead, the method presented here treats the tip and the sample as separate entities and generates a simulated STM image by translating the tip across the sample, proving to be a more efficient process. This method is appropriate in the weak-coupling limit (gap resistance $\gg R_Q \sim 20$ kΩ), where the sample does not significantly perturb the tip wave functions and vice versa.

B. Model of the tip

The tip cluster model [Fig. 2(a)] is comprised of 24 tungsten atoms with fixed coordinates derived from the bcc lattice of bulk tungsten (lattice constant 3.19 Å). The trigonal pyramidal tip consists of four layers of atoms in the (111) direction, ending in a single apex atom with a cluster symmetry of C_{3v}. Density-functional theory calculations were performed with Jaguar v4.0 using the B3LYP functional and LACVP** basis set treated with the effective core potential.[27] DFT calculations sometimes have difficulty properly converging to the ground state for transition metals due to the large number of possible electronic states available to the metal. With an extension of the pseudospectral parameters in Jaguar, the self-consistent-field (SCF) calculations of the system converged slowly, and ultimately calculated a ground state with a final iteration energy difference of 10^{-6} hartrees.

The structure of the tip cluster model was chosen for two different reasons, based on the work of Tsukada and co-workers.[29] The tunneling current is predominantly concentrated at the apex atom due to exponential decay of the wave functions of the underlying atoms. Therefore, a tip pos-

sessing a single apex atom is critical for obtaining high-resolution STM images.[29] C_{3v} symmetry is the simplest symmetry for a tip that is parallel to the [111] direction. The LDOS over an integrated energy range of 1.5 eV (from E_f -1.5 eV to E_f) in an 8 Å $\times$ 8 Å region plotted in a plane located 3 Å above the nuclear position of the apex atom is displayed in Fig. 2(b). The plot clearly displays the electron density as predominantly situated at the apex atom. A detailed analysis of the molecular orbital coefficients derived from the DFT calculations reveals that the tip wave function can be considered as a linear combination of s, p, and d atomic orbitals over the energy range $E_f-1.5$ to E_f. Additionally, the significantly increased number of atoms (previous STM simulations typically employed a single tungsten atom as the tip) yields a DOS and Fermi level comparable to bulk tungsten metal [Fig. 2(c)] while remaining within reasonable limits of current computational ability. (The DOS plot was obtained by substituting Lorentzian functions with a 0.1 eV width parameter into the delta functions of the cluster levels.[29]) Furthermore, the decay length of the evanescent wave function from the tip is approximately 1 Å. This value is considerably shorter—and more realistic—than single s-wave tip models. In summary, using the DOS and the decay length of the wave function as metrics, the tip cluster model employed in these simulations provides a more realistic model than the Tersoff-Hamann[3] s-wave tip approximation.

C. Model of the sample surface

A Si_9H_{12} cluster was employed to simulate one silicon dimer of the Si(100)-2$\times$1 surface. Density-functional theory calculations were performed using the B3LYP functional and 6–31G** basis set to obtain the electronic structure of the geometry-optimized and energy-minimized dimer cluster. The SCF calculations were allowed to converge to the final ground state. The final Si(100)-2$\times$1 surface was generated by laterally translating and tiling the Si_9H_{12} cluster dimer in accordance with Si(100)-2$\times$1 crystalline dimensions. This simplification ignores interactions between individual surface dimers, and thus affects the dimer corrugation in the final simulated image.

Density-functional theory calculations incorporating periodic boundary conditions of a bulk crystalline Si(100)-2 $\times$1 surface produce a π bonding interaction and π^* antibonding interaction below and above the sample Fermi level, respectively.[30] Similarly, DFT calculations of the Si_9H_{12} cluster derive highest occupied (HOMO) and lowest unoccupied (LUMO) molecular orbitals corresponding to the π bonding and π^* antibonding interactions. Therefore, the decay properties of the silicon dimer wave functions generated utilizing this model should not significantly deviate with such a simplification.

The molecular structures displayed in Fig. 1 were used to calculate the energies of the wave functions for both the monovertex [Fig. 1(a)] and cracked cluster [Fig. 1(b)] attachment models. The monovertex attachment model contains the following key propositions: (1) the cluster cage remains intact, (2) the cluster is activated at one of the Si-H vertices,

and (3) the cluster bonds to a Si dimer atom via a single Si-Si bond.[9–12] The cracked cluster model features Si-O bond scission along a cluster cage edge, resulting in a bridged bonding configuration across a Si dimer.[13,14] For these models, the Si_9H_{12} cluster was employed to simulate the silicon surface dimer to which the cluster is bonded. Density-functional theory calculations were performed using the B3LYP functional and the $6-31G^{**}$ basis set and the SCF calculations were allowed to converge to final ground states.[27] Spherosiloxane cluster adsorption on the Si(100)-2 $\times$ 1 surface was modeled by replacing a surface Si dimer with one of the structures in Fig. 1. Comparing simulated STM images of the clean silicon surface to a surface with a chemisorbed $H_8Si_8O_{12}$ cluster delivers a fast and reliable way to ascertain molecular adsorbate image contrast information.

For the monovertex attachment model, an important parameter to consider is the angle formed by the silicon surface and the plane encompassing the atoms in the top face of the cluster. Molecular mechanics calculations suggest the angle is $\sim 25°-30°$, as depicted in Fig. 1(a). Typically, molecular adsorption to a single Si dimer atom induces significant dimer buckling on the order of $\sim 10°-15°$.[31] Since the geometric optimization for the one-dimer substrate model does not produce dimer buckling, the face angle parameter was constrained between $5°-10°$ to account for this likely effect.

III. RESULTS

Filled- and empty-states experimental STM images of the same chemisorbed $H_8Si_8O_{12}$ spherosiloxane cluster on Si(100)-2 $\times$ 1 in a 26 Å $\times$ 26 Å region are presented in Figs. 3(a) and 3(b), respectively. Three key aspects are apparent in the filled-states image, Fig. 3(a): (1) the square formed by the four cluster features spans the dimer vacancy trench and overlaps two dimer rows, (2) the edges of this square are oriented parallel (and perpendicular) to the direction of the dimer rows, and (3) there exists a pronounced asymmetry in the brightness of the pairs of spots that run parallel to the dimer rows [evident in the line scans in Fig. 4(a)].[12] In the empty-states image of the same chemisorbed cluster, Fig. 3(b), only a single continuous oblong feature is apparent. The cluster features apparent in this experimental data provide a set of criteria by which to evaluate the proposed bonding models of the chemisorbed $H_8Si_8O_{12}$ cluster.

Consideration beyond the gross lateral features of the experimental data yields two additional geometric discrepancies, the first of which concerns the apparent height of the cluster. Both filled- and empty-states experimental STM images yield cluster apparent heights of $\sim 0.8-1.0$ Å (Fig. 4). As often observed for three-dimensional molecules, this experimentally observed apparent height is significantly less than the cluster geometric height (~ 5 Å). The second apparent discrepancy is the distance between individual cluster features (~ 5 Å) in the filled-states image. If these features arise from the oxygen lone pair electrons, as has previously been reported,[12] one may expect feature separations of ~ 2.8 Å in accordance with the actual cluster geometry. With these ideas in mind, we turn to simulation to examine the
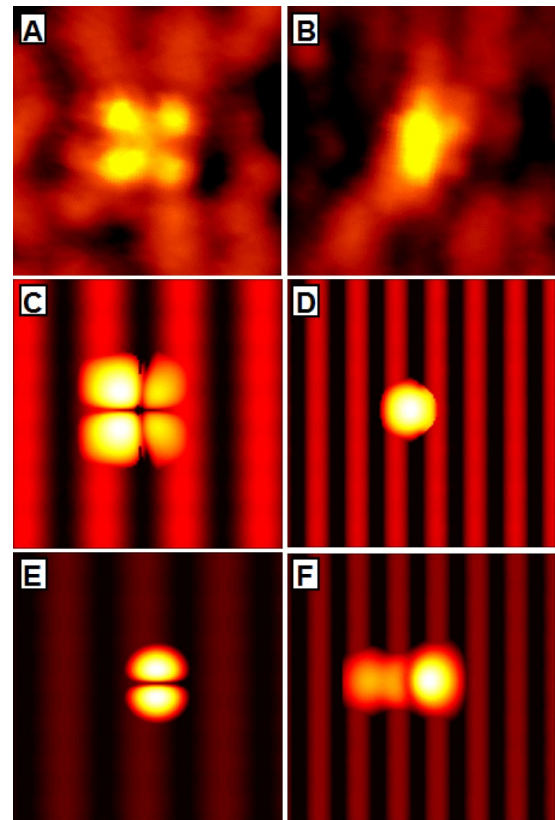

FIG. 3. (Color online) (a), (b) Experimental and (c)–(f) simulated constant current STM images of an individual $H_8Si_8O_{12}$ cluster chemisorbed to Si(100)-2 $\times$ 1. All images are in a 26 Å $\times$ 26 Å region. (a) Experimental filled-states image; $V_S = -1.5$ V, $I_T = 0.1$ nA. (b) Experimental empty-states image; $V_S = +1.5$ V, $I_T = 0.1$ nA. (c) Simulated filled-states image of a monovertex-attached $H_8Si_8O_{12}$ cluster; $V_S = -1.5$ V, $I_T = 0.5$ nA. (d) Simulated empty-states image of a monovertex-attached $H_8Si_8O_{12}$ cluster; $V_S = +1.5$ V, $I_T = 0.5$ nA. (e) Simulated filled-states image of a $H_8Si_8O_{12}$ cluster attached according to the cracked cluster model; $V_S = -1.5$ V, $I_T = 0.5$ nA. (f) Simulated empty-states image of a $H_8Si_8O_{12}$ cluster attached according to the cracked cluster model; $V_S = +1.5$ V, $I_T = 0.5$ nA. (The disorder in the Si dimer rows near the cluster is not representative of the majority of images. This figure presents simultaneously acquired filled- and empty-states images that are over a somewhat defective region of the substrate.)

two adsorption models and to understand the origin of the image features and dimensions.

Simulated STM images of the chemisorbed $H_8Si_8O_{12}$ cluster on the Si(100)-2 $\times$ 1 surface for both the monovertex [Figs. 3(c) and 3(d)] and "cracked cluster" [Fig. 3(e) and 3(f)] attachment models were generated utilizing nominally the same tunneling conditions as the actual STM experiments by the methods described above. Filled- [Figs. 3(c) and 3(e)] and empty-states [Figs. 3(d) and 3(f)] images were generated for both adsorption models. A quantitative and qualitative comparison of the simulated images to the experimental STM images is instructive. Recall, the simplification taken in substrate modeling enhances the silicon dimer corrugation in the simulated image, thus, the comparison focuses on the molecular features.
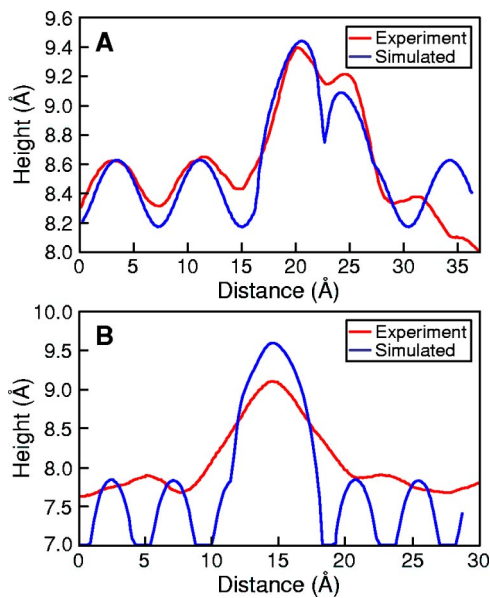
FIG. 4. (Color online) A comparison of experimental and simulated apparent cluster heights. (a) Filled-states STM image height profiles taken across a pair of cluster features oriented perpendicular to the dimer row direction in the experimental and simulated images reported in Figs. 3(a) and 3(c). (b) Empty-states STM image height profiles taken across cluster features in Figs. 3(b) and 3(d).

For filled-states STM images, electrons tunnel from the occupied states of the sample surface into the unoccupied states of the tip. Thus, filled-states STM images largely reflect the LDOS of the sample surface. Using the model described above, DFT indicates the HOMO and HOMO-1 molecular orbitals that predominantly contribute to the tunneling current. The HOMO of $H_8Si_8O_{12}$ is primarily derived from a linear combination of the oxygen $2p$ atomic orbitals.[12,32]

The filled-states STM image simulations in Figs. 3(c) and 3(e) indicate the image feature maxima are associated with cluster oxygen atoms. The simulated filled-states STM image of a $H_8Si_8O_{12}$ cluster chemisorbed according to the monovertex attachment model [Fig. 3(c)] produces four features associated with the four oxygen atoms in the top face of the cluster. Recall, the monovertex attachment model orients the cluster at an angle with respect to the underlying substrate, thus producing a pronounced asymmetry in the brightness of the pairs of cluster features. In contrast, the simulated filled-states STM image of a $H_8Si_8O_{12}$ cluster chemisorbed according to the cracked cluster model [Fig. 3(e)] displays two large features corresponding to the molecular orbital dominated by the $2p$ atomic orbital of the top oxygen atom.

Lastly, there is a significant difference in the apparent cluster height between the simulated STM images of the two adsorption models. The monovertex and cracked cluster attachment models yield apparent cluster heights of ~ 1 and ~ 3 Å, respectively. The disparity in apparent heights is likely a result of the differing geometric arrangements of the cluster relative to the underlying substrate. Recall, the face angle parameter of the monovertex-attached cluster was constrained between $5° - 10°$. This places the oxygen atoms in the top face of the cluster ~ 5 Å above the silicon surface

whereas the topmost oxygen atom in the cracked cluster model is ~ 7 Å above the silicon surface.

For empty-states STM images, electrons tunnel from the occupied states of the tip into the unoccupied states of the sample surface. Thus, empty-states STM images largely reflect the LDOS of the unoccupied electronic states of the sample surface. Density-functional theory calculations of $H_8Si_8O_{12}$ indicate the cluster LUMO is predominantly delocalized inside the spherosiloxane cage.[12,32] A simulated empty-states STM image of a $H_8Si_8O_{12}$ cluster chemisorbed according to the monovertex attachment model [Fig. 3(d)] yields one continuous bright surface protrusion largely corresponding to the electron density of the delocalized cluster LUMO. However, a simulated empty-states STM image of a $H_8Si_8O_{12}$ cluster chemisorbed according to the cracked cluster attachment model [Fig. 3(f)], yields a region containing one dominant, bright feature and two less intense features corresponding to the electron density around the O, Si, and H atoms, respectively, located at the top cluster edge. In addition, the apparent cluster heights for the two adsorption models display a similar 2 Å difference, as previously discussed for the simulated filled-states images.

Through both qualitative and quantitative comparisons of the simulated STM images in Figs. 3(c)–3(f) to the experimental STM images in Figs. 3(a) and 3(b), one can conclude $H_8Si_8O_{12}$ spherosiloxane clusters preferentially chemisorb to the Si(100)-2×1 surface in accordance with the monovertex attachment model. The simulated filled-states STM image of a cluster chemisorbed according to the monovertex attachment model is consistent with all three key features apparent in the experimental data: (1) the square formed by the four cluster features spans the dimer vacancy trench and overlaps two dimer rows, (2) the edges of this square are oriented parallel and perpendicular to the direction of the dimer rows, and (3) the pronounced asymmetry in the brightness of the pairs of spots that run parallel to the dimer row direction. The simulated filled-states STM image of a cluster chemisorbed according to the cracked cluster model is inconsistent with all three of these observations. Finally, the apparent heights of the cluster features in the simulated images of a cluster chemisorbed according to the monovertex attachment model are nearly equivalent to those observed in the experimental STM data (Fig. 4). However, the apparent heights of the cluster features in the simulated images of a cluster chemisorbed according to the cracked cluster model are nearly 200% greater than what is experimentally observed.

In addition to the above analysis regarding the preferred cluster binding mode, the simulation of the monovertex binding accurately predicts the apparent discrepancy between cluster features, as observed in the experimental data with respect to the actual cluster geometry. The $H_8Si_8O_{12}$ spherosiloxane cluster geometry suggests that a height of ~ 5 Å should be experimentally measured; whereas the simulated apparent heights very closely match the experimentally observed apparent heights of $\sim 0.8 - 1.0$ Å. In addition, the exaggerated distance between oxygen atoms in the top face of the cluster observed in the experimental filled-states image is also reproduced in the simulated filled-states image.

Concerning the cluster height, recall that the monovertex attachment model orients oxygen atoms in the top face of the
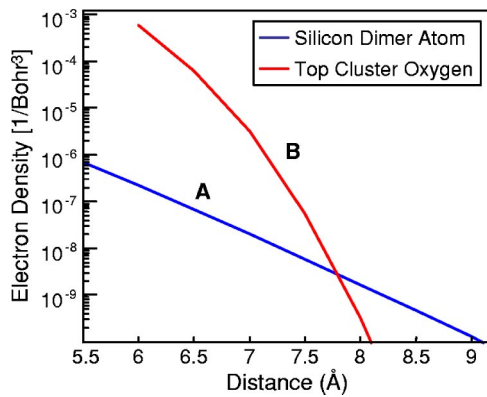
FIG. 5. (Color online) Calculated LDOS as a function of increasing distance normal to the Si(100)-2×1 surface for the monovertex-attached $H_8Si_8O_{12}$ cluster. The origin of the x-axis indicates the position of the silicon dimer atom in part (a). (a) LDOS of a silicon dimer atom. (b) LDOS of a top face $H_8Si_8O_{12}$ cluster oxygen atom.

cluster ~5 Å away from the underlying substrate. Taking this height differential into account, one may naively conclude the wave functions associated with the cluster oxygen atoms protrude farther into the vacuum than that of the underlying silicon dimer atoms, and thus preserve the ~5 Å height differential. Examining the radial extent of the LDOS of the chemisorbed cluster oxygen atoms and the underlying substrate Si atoms reveals the origin of this discrepancy. Figure 5 displays the LDOS of a surface silicon dimer atom [Fig. 5(a)] and an oxygen atom in the top face of a monovertex-attached $H_8Si_8O_{12}$ cluster [Fig. 5(b)] plotted as a function of increasing distance normal to the Si(100)-2×1 surface (LDOS values were calculated for an integrated energy range within 1.5 eV of the HOMO). The LDOS of the cluster oxygen atoms clearly decay much faster than that of the underlying silicon dimer atoms. As a result of the disparity in wave-function decay lengths, the oxygen atoms in the top cluster face (predominantly responsible for generating the features observed in the filled-states STM image) would yield an apparent cluster height significantly less than the actual cluster geometric dimensions. Indeed, this physical effect is observed in both the experimental and simulated STM images.

Finally, the origin of the discrepancy in the lateral extent of cluster features warrants explanation. This effect is a consequence of the wavelike interaction between the tip and the sample, giving rise to tunneling. Two manifestations are readily apparent in the simulated STM images presented in this paper. The first exaggerates the separation distance if the phase of the molecular orbital changes over the region scanned. The second entails a loss of resolution by not discriminating within the molecular orbitals consisting of a single phase. Figure 6 illustrates these effects using artificially generated wave functions (all simulated images are plotted in an 8 Å×8 Å region). Figure 6(a) displays a molecular orbital consisting of two s-type atomic orbitals of dissimilar phases separated by a distance of 2 Å, as observed at a plane 3 Å above the nuclear cores with the positive and negative phases colored red and blue, respectively. However,
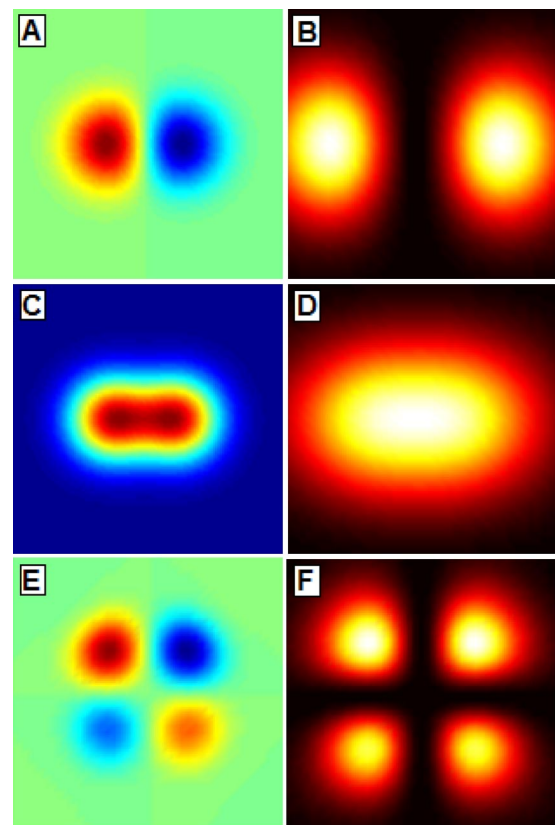

FIG. 6. (Color online) An investigation of STM convolution effects. All images are plotted in an 8 Å×8 Å region. (a) displays a molecular orbital consisting of two s-type atomic orbitals of dissimilar phases separated by a distance of 2 Å as observed at a plane 3 Å above the nuclear cores with positive and negative phases colored red and blue, respectively. (b) Simulated constant height STM image of part (a). (c) displays a molecular orbital consisting of two s-type atomic orbitals of the same phase separated by a distance of 2 Å as observed at a plane 3 Å above the nuclear cores. (d) Simulated constant height STM image of part (c). (e) The molecular orbital of a monovertex-attached cluster as observed at a plane 2 Å above the oxygen atoms in the top face of the cluster. (f) Simulated constant height STM image of part (e).

a simulated constant height image of this surface, Fig. 6(b), displays two image maxima separated by a distance of ~5 Å. This effect is best understood by realizing that the matrix element for electron transfer involves an integral over the spatially extended wave functions of the tip and sample. In the area near the transition of the sample wave-function phase, the matrix element is reduced due to the contributions from oppositely phased regions. This suppresses the tunneling current and moves the current maxima outward away from the transition region, yielding an image with a larger apparent spacing between features than is actually present on the surface. The converse effect is present when wave functions of similar phases are separated by a node. A molecular orbital consisting of two s-type atomic orbitals of the same phase separated by a distance of 2 Å as observed at a plane 3 Å above the nuclear cores is displayed in Fig. 6(c) with the corresponding simulated STM image displayed in Fig. 6(d). Note the individual atomic orbitals making up the molecular

orbital are no longer separately resolved in the simulated image. This effect is dependent upon the lateral extent of the STM tip wave function, i.e., the tip "sharpness," as well as on the separation distance between the molecular orbital features.

It is further instructive to consider these effects with respect to the $H_8Si_8O_{12}$ molecule. The molecular orbital observed at a plane 2 Å above the oxygen atoms in the top face of a monovertex-attached cluster is displayed in Fig. 6(e). Recall that DFT calculations indicate the first four low-lying occupied molecular orbitals are localized on the oxygen and derived from $2p$ lone pair electrons separated by a distance of ~ 2.8 Å. As previously demonstrated in Figs. 6(a) and 6(b), a simulated constant height image of the cluster yields an exaggerated separation (~ 5 Å) between features of the $H_8Si_8O_{12}$ spherosiloxane cluster. This agrees well with the observed feature separation displayed in the experimental filled-states STM image [Fig. 3(a)].

IV. SUMMARY AND CONCLUSIONS

Simulated STM images were calculated using a simulation method based on Bardeen's tunneling formalism. The method was employed to simulate a three-dimensional $H_8Si_8O_{12}$ spherosiloxane cluster chemisorbed to the Si(100)-2×1 surface. A comparison of the theoretical and experimental data confirm that $H_8Si_8O_{12}$ clusters preferentially chemisorb to Si(100)-2×1 in accordance with the monovertex bonding model. In addition, the simulations elucidate the cause of discrepancies frequently observed in the apparent vertical and lateral dimensions (relative to geometric molecular dimensions) in STM images of molecular adsorbates.

[1] P. S. Weiss and D. M. Eigler, Phys. Rev. Lett. **71**, 3139 (1993).

[2] J. Bardeen, Phys. Rev. Lett. **6**, 57 (1961).

[3] J. Tersoff and D. R. Hamann, Phys. Rev. B **31**, 805 (1985).

[4] C. J. Chen, Phys. Rev. B **42**, 8841 (1990).

[5] W. A. Hofer and J. Redinger, Surf. Sci. **447**, 51 (2000).

[6] W. A. Hofer, A. J. Fisher, and R. A. Wolkow, Surf. Sci. **475**, 83 (2001).

[7] P. Sautet, Chem. Rev. **97**, 1097 (1997).

[8] J. Crystal, L. Y. Zhang, R. A. Friesner, and G. W. Flynn, J. Phys. Chem. A **106**, 1802 (2002).

[9] M. M. Banaszak Holl and F. R. McFeely, Phys. Rev. Lett. **71**, 2441 (1993).

[10] S. Lee, S. Makan, M. M. Banaszak Holl, and F. R. McFeely, J. Am. Chem. Soc. **116**, 11819 (1994).

[11] J. N. Greeley, L. M. Meeuwenberg, and M. M. Banaszak Holl, J. Am. Chem. Soc. **120**, 7776 (1998).

[12] K. S. Schneider, Z. Zhang, M. M. Banaszak Holl, B. G. Orr, and U. C. Pernisz, Phys. Rev. Lett. **85**, 602 (2000).

[13] K. Raghavachari and J. Eng, Phys. Rev. Lett. **84**, 935 (2000).

[14] K. Raghavachari, A. Pasquarello, J. Eng, and M. S. Hybertsen, Appl. Phys. Lett. **76**, 3873 (2000).

[15] H. N Waltenburg and J. T. Yates, Chem. Rev. **95**, 1589 (1995).

[16] R. J. Hamers and Y. J. Wang, Chem. Rev. **96**, 1261 (1996).

[17] P. A. Agaskar, Inorg. Chem. **30**, 2707 (1991).

[18] P. A. Agaskar and W. G. Klemperer, Inorg. Chim. Acta **229**, 355 (1995).

[19] R. H. Baney, M. Itoh, A. Sakakibara, and T. Suzuki, Chem. Rev. **95**, 1409 (1995).

[20] K. T. Nicholson and M. M. Banaszak Holl, Phys. Rev. B **64**, 155317 (2001).

[21] J. Shoemaker, L. W. Burggraf, and M. S. Gordon, J. Chem. Phys. **112**, 2994 (2000).

[22] T. D. Crawford, J. F. Stanton, J. C. Saeh, and H. F. Schaefer, J. Am. Chem. Soc. **121**, 1902 (1999).

[23] R. A. King, T. D. Crawford, J. F. Stanton, and H. F. Schaefer, J. Am. Chem. Soc. **121**, 10788 (1999).

[24] M. M. Banaszak Holl, S. H. Lee, and F. R. McFeely, Appl. Phys. Lett. **65**, 1097 (1994).

[25] F. R. McFeely, K. Z. Zhang, M. M. Banaszak Holl, S. H. Lee, and J. E. Bender, J. Vac. Sci. Technol. B **14**, 2824 (1996).

[26] W. C. Simpson, J. A. Yarmoff, W. H. Hung, and F. R. McFeely, Surf. Sci. **355**, L283 (1996).

[27] Jaguar 4.0; Schrödinger, 1500 S.W. First Ave., Suite 1180, Portland, OR 97201.

[28] G. Orlandi, A. Troisi, and F. Zerbetto, J. Am. Chem. Soc. **121**, 5392 (1999).

[29] M. Tsukada, K. Kobayashi, and N. Isshiki, Surf. Sci. **242**, 12 (1991).

[30] J. Dabrowski and M. Scheffler, Appl. Surf. Sci. **56**, 15 (1992).

[31] R. J. Hamers, R. M. Tromp, and J. E. Demuth, Phys. Rev. B **34**, 5343 (1986).

[32] K. H. Xiang, R. Pandey, U. C. Pernisz, and C. Freeman, J. Phys. Chem. B **102**, 8704 (1998).